CHEMISTRY
A EUROPEAN JOURNAL

DOI: 10.1002/chem.201001650

Molecular Alloys: Experimental and Theoretical Investigations on the Substitution of Zinc by Cadmium and Mercury in the Homologous Series $[Mo(M'R)_{12}]$ and $[M(M'R)_8]$ (M = Pd, Pt; M′ = Zn, Cd, Hg)**

Timo Bollermann,[a] Thomas Cadenbach,[a] Christian Gemel,[a] Moritz von Hopffgarten,[b] Gernot Frenking,*[b] and Roland A. Fischer*[a]

Abstract: The synthesis and structural characterization of novel, metal-rich, highly coordinated compounds $[Mo(M'R)_{12}]$ and $[M(M'R)_8]$ (M: Pd, Pt, Mo; M′: Zn, Cd; R: Me = CH_3, Cp* = pentamethylcyclopentadienyl) are reported. Additionally, a description of the bonding situation of the new compounds by means of quantum-chemical calculations is presented including the Hg analogues. Reaction of $[Pt(GaCp^*)_4]$ with $CdMe_2$ results in the formation of the unprecedented all-Cd coordinated $[Pt(CdMe)_4(CdCp^*)_4]$ (**1**). Similarly, the treatment of the all-Zn coordinated $[Pd(ZnMe)_4(ZnCp^*)_4]$ with $CdMe_2$ affords the novel Zn/Cd mixed compound $[Pd(CdMe)_4(ZnCp^*)_4]$ (**2**). The related Zn/Cd mixed compound $[Mo(ZnCp^*)_3(CdMe)_9]$ (**3**) is prepared by reaction of $[Mo(ZnCp^*)_4(GaMe)_4]$ with an excess amount of $CdMe_2$. All compounds were analyzed by ^1H and ^{13}C NMR spectroscopy, elemental analysis, and single-crystal X-ray diffraction. The bonding situation of these highly coordinated, metal-rich molecules **1–3** were studied by quantum-chemical calculations using density functional theory (DFT) at the BP86/TZ2P+ level, atoms-in-molecules (AIM) analysis, and energy-decomposition analysis (EDA), as well as the its natural orbitals for chemical valence variation (EDA-NOCV) and including the hypothetically all-Hg-coordinated analogues. The results point out that the radial interactions M–M′ in the icosahedral compounds that have twelve ligands are best described as classical electron-pair-sharing covalent bonds, whereas the dodecahedral species, which have eight ligands, exhibit metal–ligand donor–acceptor bonds. The attractive interactions between the metal–ligand fragments M′R by means of M′–M′ bonds are weaker but not insignificant. All complexes fulfill the 18-electron rule. The analysis clarifies the electronic structures as being distinctly different from typical endohedral clusters $M@(M''R)_n$ that exhibit strong peripheral M″–M″ interactions: The M′–M′ bonds are not strong enough to yield stable $(M'R)_n$ cages.

Keywords: bonding analysis · cadmium · cluster compounds · coordination compounds · zinc

Introduction

In the course of the investigations on the coordination chemistry of monovalent organo Group 13 compounds ER (E = Al, G, In; R = bulky substituents, in particular using $Cp^* = C_5Me_5$) at transition-metal centers M,[1] we recently discovered an unprecedented family of metal-rich compounds of the general formula $[M(ZnR)_n]$ ($n \geq 8$; M = Mo, Ru, Rh; Ni, Pd, Pt; R = CH_3, Cp*).[2] The unique access to these novel compounds is based on combined Ga/Zn and Cp*/Me exchange reactions when homoleptic starting compounds of the type $[M(GaCp^*)_{n/2}]$, are treated with a solution of $ZnMe_2$ (or $ZnEt_2$) in toluene. The monovalent organometallic zinc fragments ZnR (R = CH_3, Et, Cp*) turned out to be surprisingly versatile in strongly binding to various

[a] T. Bollermann, Dr. T. Cadenbach, Dr. C. Gemel, Prof. Dr. R. A. Fischer
Inorganic Chemistry II: Organometallics & Materials
Faculty of Chemistry and Biochemistry
Ruhr, University Bochum, 44870 Bochum (Germany)
Fax: (+49) 234-321-4174
E-mail: roland.fischer@rub.de

[b] M. von Hopffgarten, Prof. Dr. G. Frenking
Department of Chemistry, Philipps-University Marburg
35032 Marburg (Germany)
Fax: (+49) 6421-2825566
E-mail: frenking@chemie.uni-marburg.de

[**] Organo Group 13 complexes of d-block elements LIX.

Supporting information for this article is available on the WWW under http://dx.doi.org/10.1002/chem.201001650.

transition metals across Group 6 to Group 10 of the periodic table and act as purely one-electron ligands that allow for unusually high coordination numbers (CN) ≥ 8 at the transition-metal center (Figure 1).

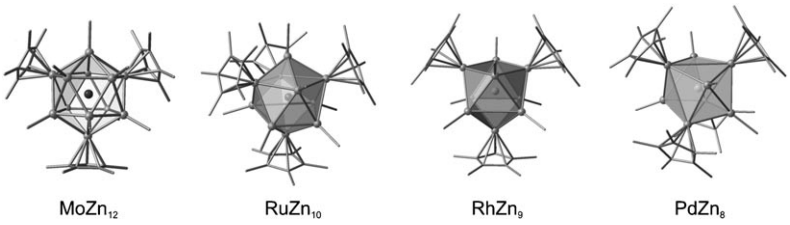

Figure 1. Molecular structures of the prototypes of the novel series of metal-rich molecules of the general formula $[M(Zn'R)_n]$ ($n \geq 8$; M = Mo, Ru, Rh; Ni, Pd, Pt; R = CH_3, Cp*).[2]

The structural properties determined by single-crystal X-ray diffraction and the theoretical bonding analysis of a selection of prototypes of the series—for example, the icosahedral molecule $[Mo(ZnCp^*)_3(ZnMe)_9]$ or the slightly distorted trigonal dodecahedral molecule $[Pd(ZnCp^*)_4(ZnMe)_4]$—suggested these compounds for consideration as new links between M/Zn coordination compounds and mixed-metal molecular clusters on the one hand and the respective solid-state intermetallic phases, that is, Hume-Rothery-type alloys, on the other (Figure 1).[2] Interestingly, the bonding analysis of the above examples revealed that the tangential Zn–Zn interactions are far less important to the overall stability of these molecules than the radial M–Zn bonds. Thus, these apparently cagelike molecules are in fact particularly different from known interstitial intermetalloid Zintl-type clusters.[3] The high thermal stability together with the strict validity of the eighteen-electron rule as a heuristic guideline for the synthesis of these new compounds supports the idea of extending the concept to a general series of monovalent organometallic species M′R (M′ = Mg; Cd, Hg; Al, Ga, In; Sn, Pb, and so on). These fragments are likely to act as one-, two-, or three-electron ligands, and in some cases, with their actual steric and bonding properties being comparable to ZnR, the mixed-metal compounds $[M(M'R^1)_a(M''R^2)_b]$ (M = d metal) may be stable. Clearly, this is true for M′ = Ga; $R^1 = CH_3$, because Ga/Zn mixed-metal compounds such as $[Mo(ZnCp^*)_4(GaMe)_4]$ are already known.[2] Following this line of reasoning, we explored the possibility of obtaining the cadmium analogues or the mixed Zn/Cd analogues of the above-mentioned prototypes, namely, $[Mo(ZnR^1)_{12-n}(CdR^2)_n]$ ($n \leq 12$) and $[M(ZnR)_{8-n}(CdR')_n]$ ($n \leq 8$; M = Pd, Pt), with R^1 and R^2 being CH_3 or Cp*, respectively. Because of the highly toxic nature of mercury compounds, that is, $HgMe_2$, which are unavoidable for a successful synthesis of the mercury-containing derivatives, we restricted ourselves to the Cd chemistry but included related Hg model compounds in the quantum-chemical calculations and the comparative theoretical characterization of the homologous series $[M(M'R^1)_a(M''R^2)_b]$ (M = Mo, Pd, Pt; $a+b = 12, 8$; M′ = Zn, Cd, Hg) as mentioned in the title.

Results and Discussion

Synthesis, properties, and structural characterization: In analogy to the preparation of $[Mo(ZnCp^*)_3(ZnMe)_9]$ from $[Mo(GaCp^*)_6]$ and $ZnMe_2$ or $[M(ZnCp^*)_4(ZnMe)_4]$ (M = Ni, Pd, Pt) from $[M(GaCp^*)_4]$ and $ZnMe_2$, the reaction of the homoleptic compound $[Pt(GaCp^*)_4]$ with an excess amount of $CdMe_2$ in toluene at reflux leads to the formation of the new homoleptic $PtCd_8$ compound $[Pt(CdCp^*)_4(CdMe)_4]$ (**1**) in isolated yields around 50% (Scheme 1). Experiments

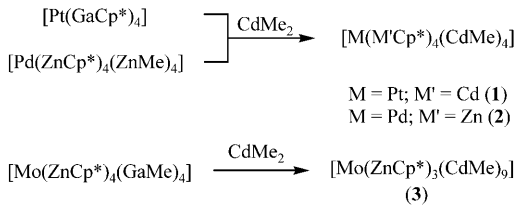

Scheme 1. Preparation of the new compounds **1**, **2**, and **3**.

with less than stoichiometric amounts of $CdMe_2$ to afford mixed Cd/Ga species have not yet been performed but are likely to be successful due to the existence of $[Mo(ZnCp^*)_4(GaMe)_4]$. Compound **1** dissolves well in nonpolar solvents such as benzene or hexane and is quite stable when stored under an inert gas atmosphere as a solid, whereas slow decomposition occurs in solution, even at −30 °C. The compound crystallizes in the triclinic space group $P\bar{1}$ with four molecules in the unit cell. The molecular structure (Figure 2) as determined by single-crystal X-ray diffraction exhibits the platinum atom in a distorted square-antiprismatic coordination geometry comparable to the isovalent electronic cation $[Pt(AuPPh_3)_8]^{2+}$ rather than a trigonal dodecahedral.[4] The Cp* groups are symmetrically coordinated

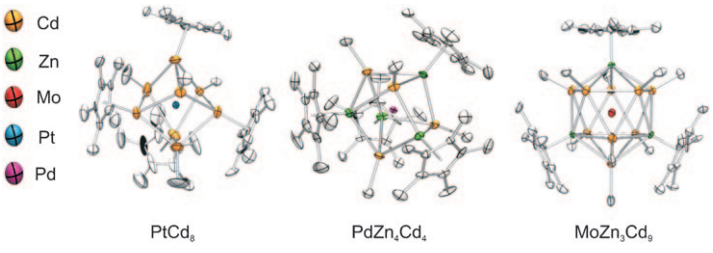

Figure 2. Molecular structures of $[Pt(CdCp^*)_4(CdMe)_4]$ (**1**), $[Pd(ZnCp^*)_4(CdMe)_4]$ (**2**), and $[Mo(ZnCp^*)_3(CdMe)_9]$ (**3**) as determined by single-crystal X-ray crystallography (thermal ellipsoids are shown at the 50% probability level, hydrogen atoms have been omitted for clarity). Important interatomic distances [Å] are summarized in Table S1 in the Supporting Information.

in a η^5-fashion to the Cd atoms, with an average value of 2.206 Å, and the Cd–CH_3 bond lengths lie between 2.116(10) and 2.162(8) Å, which is clearly longer than the Cd–CH_3 bond length in [{η^3-HB(3-*t*Bu-5-Mepz)$_3$}$CdCH_3$] (2.074(19) Å; 3-*t*Bu-5-Mepz = 3-*tert*-butyl-5-methyl-1-pyrazolyl), the shortest Cd–CH_3 bond length in the literature but otherwise between the average distances for Cd–CH_3 found in the literature.[5] For the Cd–Cp* unit, suitable literature date for comparison are lacking. The eight Pt–Cd distances are almost equal within the narrow range of 2.6202(8)–2.6267(7) Å for Pt–CdMe and 2.6055(7)–2.6178(7) Å for Pt–CdCp*. In addition to solid-state Pt/Cd intermetallic phases such as Pt_3Cd_1 and Pt_1Cd_5 (typical distances are between 2.5852 and 2.8909 Å for Pt–Cd and 2.8143 and 3.0052 Å for Cd–Cd),[6] there are only a few known molecular compounds with direct covalent Pt–Cd interactions. The documented Pt–Cd bonds in these molecular compounds range between 2.6101(8) Å for [{$Pt(CH_3)_2$(bpy)}{Cd(cyclen)}]$(ClO_4)_2$ (bpy = 2,2′-bipyridyl; cyclen = 1,4,7,10-tetraazacyclododecane) to 3.2509(15) Å for [Pt_4Cd_6(C≡CPh)$_4$(μ-C≡CPh)$_{12}$(μ$_3$-OH)$_4$]).[7,8] Notably, the structural motif of an all-Cd octacoordinated Pt center, $PtCd_8$, is unknown in molecules to date, whereas structural motifs with higher coordination numbers are observed in solid-state compounds.[6] The tangential Cd–Cd distances in **1** vary between 3.0422(10) and 3.4099(10) Å, and these values indicate quite weak Cd–Cd interactions. The comparably stable Cd_2^{2+} ion exhibits a much stronger covalent Cd–Cd σ bond and consequently shows a quite close Cd–Cd contact (e.g., 2.576 Å in [$Cd_2(AlCl_4)_2$]).[9] The ^{1}H NMR spectrum of **1** at room temperature in C_6D_6 is very simple and gives rise to only two singlets at $\delta = 0.03$ ppm (12 H; $CdCH_3$) and $\delta =$ 2.19 ppm (60 H; CdC_5Me_5), respectively. The ^{13}C NMR spectrum displays the expected resonances for the methyl groups at $\delta = 19.72$ ppm as well as the signals for the Cp* unit at $\delta = 11.03$ ppm (CdC_5Me_5) and $\delta = 112.21$ ppm (CdC_5Me_5). ^{195}Pt and ^{113}Cd NMR spectroscopic studies turned out to be difficult because of the instability of **1** in solution and will be presented elsewhere.

As we already discussed for the synthesis of the parent molecule [$Mo(ZnCp^*)_3(ZnMe)_9$],[2] the role of the GaCp* ligands in the starting compounds of Scheme 1, at least conceptually, includes the formal reduction of the $CdMe_2$ from Cd^{II} to Cd^{I} over the course of the reaction. Certainly, the assignment of formal oxidation states M^0 and M'^{I} is ambiguous for these kind of molecules. We discussed this issue previously in some detail.[2] Nevertheless, we found $GaMe_3$ as the major gallium-containing byproduct, which hints toward the involvement of electron-transfer (redox) and/or radical reactions. The coordination number (CN) of the central platinum atom increases from 4 to 8, since each GaR moiety is substituted by two CdR fragments. Right away the question arises whether or not a Zn/Cd exchange reaction similar to the above-described Ga/Zn and the homologous Ga/Cd exchange is possible. Indeed, treatment of [$Pd(ZnCp^*)_4(ZnMe)_4$] with an excess amount of $CdMe_2$ selectively leads to the formation of the new Zn/Cd mixed complex [$Pd(ZnCp^*)_4(CdMe)_4$] (**2**) in preparative yields around 45% (Scheme 1). However, we have so far failed in isolating any other defined product with a different Zn/Cd ratio. Also, the homoleptic $PdCd_8$ analogue of **1** was not derived by variation of the conditions and the amount of $CdMe_2$. As discussed below, the Zn atoms of **2** selectively coordinate the Cp* moieties. We suggest that this feature points to a thermodynamic reason for the preferred stability of **2** over other possible isomers and analogous Zn/Cd mixed derivatives. Since there are no known solid-state structures of Cd–Cp* compounds as well as no thermodynamic data (bond energies), this assumption can not be confirmed by experimental data; however, the preferable binding of Cp* to Zn is observed for both **2** and **3**. Nevertheless, the existence of the homoleptic $PtCd_8$ compound **1** suggests that the related $PdCd_8$ compound may be stable as well and is likely to accessible by combining [$Pd(GaCp^*)_4$] or [$Pd_3(InCp^*)_8$][10] with $CdMe_2$ under suitable conditions.

Compound **2** dissolves well in nonpolar solvents like toluene or hexane and is distinctly more stable than **1** when stored under an inert gas atmosphere at −30 °C. The assignment of the ^{1}H and ^{13}C NMR spectroscopic data (see the Experimental Section) to the organic substituents at Zn and Cd is possible by comparison with reference compounds that exhibit ZnCp* and CdCp* moieties,[2] and matches with the solid-state structure. Compound **2** crystallizes in the orthorhombic space group $P2_12_12_1$ with four molecules in the unit cell. The molecular structure of this compound as determined by single-crystal X-ray diffraction (Figure 2) shows quite a similar coordination structure to compound **1**, that is, a trigonal dodecahedral $PdZn_4Cd_4$ metal core with the Cp* units coordinating the Zn atoms and the methyl groups located at the cadmium atoms, thus resulting in superimposition of Zn_4 and Cd_4 tetrahedra. The Cp* groups are symmetrically coordinated in a η^5 fashion to the Zn atoms, with an average value of 1.940 Å that matches typical literature data for the Zn–Cp*(centroid) distance.[2] Quite similar to **1**, the Cd–CH_3 bond lengths of 2.127(8)–2.161(5) Å are as expected.[5] The Pd–Cd distances are in the range of 2.6005(7)–2.6046(5) Å, which are much shorter than in the acetate-bridged Cd^{II}–Pd^{II} complex [$CdPd(CH_3COO)_4$]·x CH_3COOH (2.806(1) Å), a typical example of the few existing molecular Pd/Cd compounds, yet without a covalent Pd–Cd bond character.[11] The Pd–Zn distances are all very similar (2.4532(7)–2.4574(7) Å) and highly comparable to those in the starting compound [$Pd(ZnCp^*)_4(ZnMe)_4$] (2.415(1)–2.458(1) Å); they are, however, slightly longer than in the low-coordinate $PdZn_2$ complex (^{F}PNP)Pd-Zn-Pd(^{F}PNP) with direct two-electron two-center covalent Pd–Zn bonds of 2.372(1)–2.379(1) Å).[12] The distances between the Zn and Cd atoms vary between 2.9335(8) and 3.0415(10) Å, and the average values of the Zn–Zn and Cd–Cd distances are 3.995 and 4.218 Å, respectively. These distances are significantly longer than in the σ-bonded molecule Cp*ZnZnCp*.[13] For compounds RCdCdR, no experimental data are available. However this suggests only weak M–M bonding interactions in the metal cage of **2** (vide infra).

The reaction of $CdMe_2$ with $[Mo(GaCp^*)_6]$ leads to a mixture of several products that unfortunately could not be separated from each other and isolated in pure crystalline form. Nevertheless, the treatment of the mixed Ga^I/Zn^I complex $[Mo(ZnCp^*)_4(GaMe)_4]$ with an excess amount of $CdMe_2$ leads to the formation of the Zn/Cd mixed $MoZn_3Cd_9$ complex $[Mo(ZnCp^*)_3(CdMe)_9]$ (**3**) (Scheme 1). The new $MoZn_3Cd_9$ compound **3** dissolves well in nonpolar solvents like toluene or hexane and is quite stable when stored under an inert gas atmosphere at −30 °C but some decomposition takes place in solution at room temperature. It crystallizes in the triclinic space group $P\bar{1}$ with two molecules in the unit cell. The single-crystal X-ray structure determination of **3** (Figure 1) reveals an icosahedral environment of the central molybdenum atom by three ZnCp* and nine CdMe ligands, which is very similar to the structure of $[Mo(ZnCp^*)_3(ZnMe)_9]$. It should be noted that the differences in electron densities and X-ray scattering power of Zn/Ga versus Cd/Ga and Zn/Cd vary and therefore the Cd atoms can be easily located in solid-state structures. In both icosahedral compounds, the sterically demanding Cp* groups are located as far as possible from each other, thereby resulting in an overall C_3 symmetry of the molecule. The ^1H and ^{13}C NMR spectra of **3** in C_6D_6 at room temperature agree very well with the single-crystal X-ray structure and display only one signal for the chemically equivalent ZnCp* units as well as the expected three sets of methyl groups of $CdCH_3$ ligand. The Mo−Zn/Cd distances are all nearly equal, with 2.7041(14)–2.7256(15) Å for Mo−ZnCp* and 2.8576(12)–2.8864(13) Å for Mo−CdMe. Interestingly, the Mo−Zn distances are slightly elongated with respect to $[Mo(ZnCp^*)_3(ZnMe)_9]$ (2.636(9)–2.677(13) Å), which is likely to be caused by adopting the increased steric demand of the Cd atoms. To the best of our knowledge, there is no known X-ray single-crystal structure for molecular compounds with covalent Mo−Cd bonds, although the structures of $[Cp_2Mo(SnPPh_3)]_2Cd$ and *mer*-$[\{(OMe)_3Si\}(OC)_3Fe\{\mu\text{-}(Ph_2P)C_5H_4N\}Cd\{Mo(C_5H_5)\text{-}(CO)_3\}]$ have been deduced from FTIR and NMR spectroscopic data as well as elemental analysis.[14] The Cd−Cd distances of **3** (3.0018(13)–3.0570(11) Å) are again distinctly longer than in Cd_2^{2+} (2.576 Å in $[Cd_2(AlCl_4)_2]$), which points to only weak Cd−Cd interaction in the cage of **3**. The Zn−Cd distances vary between 2.9026(14)–2.9629(14) Å, which is slightly shorter in comparison to compound **2** (2.9487(10) and 3.0415(11) Å).

The data presented and discussed above clearly show that Cd-substituted analogues of the previously known Zn compounds (Figure 1) are experimentally accessible, with the homoleptic compound $[Pt(CdCp^*)_4(CdMe)_4]$ (**1**) being the key example. Interestingly, it turned out to be difficult to isolate Cd/Ga mixed compounds in a pure form, but their existence in solution is likely. In particular, novel Zn/Cd mixed compounds **2** and **3** were synthesized and nicely show the possibility of substituting Zn with Cd in the coordination sphere at the Mo or Pd center. The icosahedral, fully Cd-substituted $[Mo(CdCp^*)_3(CdCH_3)_9]$ could not be isolated in a pure form or confirmed spectroscopically. From this preparative work, we conclude that the thermodynamic stability of the Cd-substituted compounds is rapidly decreasing with an increasing amount of Cd in the product molecule. In the following section, quantum-chemical calculations on a selection of representative model compounds are presented and discussed to characterize the trends in structure, bonding situation, and stability within the homologous series of $[M(M'R)_n]$. This includes the Hg analogues, which we did not attempt to synthesize because of the extremely toxic nature of $HgMe_2$ and related reagents.

Quantum-chemical calculations: To better understand the nature of the bonding between the central atoms Pd, Pt, and Mo, and the Zn and Cd ligands, we carried out quantum-chemical calculations using density functional theory (DFT) at the BP86/TZ2P+ level (see the Experimental Section for details). In a first step we optimized gas-phase model structures of the synthesized molecules **1**–**3** in which we replaced the Cp* moieties with Cp (C_5H_5). The calculated geometries of the model compounds are in good agreement with the results of the crystal-structure analysis (see Table S1 in the Supporting Information). Next we optimized geometries of parent systems of **1**–**3** in which we replaced the organic moieties CH_3 and Cp* by hydrogen in $[Pt(CdH)_8]$ (**1H**), $[Pd(CdH)_4(ZnH)_4]$ (**2H**), and $[Mo(CdH)_9(ZnH)_3]$ (**3H**). As the calculated M−M′ distances of the latter species are in good agreement with those in the synthesized systems (see Table 1), we used these parent systems **1H**–**3H** for the bonding analyses. To extend the studies, we also calculated several homoleptic model systems with coordination number of eight, that is, $[Pd(ZnH)_8]$ (**4H**), $[Pd(CdH)_8]$ (**5H**), $[Pd(HgH)_8]$ (**6H**), $[Pt(ZnH)_8]$ (**7H**), and $[Pt(HgH)_8]$ (**8H**), and with coordination number twelve (i.e., $[Mo(ZnH)_{12}]$ (**9H**), $[Mo(CdH)_{12}]$ (**10H**), and $[Mo(HgH)_{12}]$

Table 1. Calculated bond lengths [Å] at the BP86/TZ2P+ level of the investigated model compounds **1H**–**11H**.

	E	E′	*d*(M−E)	*d*(M−E′)	*d*(E−E)	*d*(E−E′)	*d*(E′−E′)
$[Pd(CdH)_4(ZnH)_4]$ (**2H**)	Cd	Zn	2.664–2.665	2.473	3.948	2.920	3.025; 3.145
$[Pd(ZnH)_8]$ (**4H**)	Zn		2.475		2.929		
$[Pd(CdH)_8]$ (**5H**)	Cd		2.669		3.159		
$[Pd(HgH)_8]$ (**6H**)	Hg		2.693		3.174		
$[Pt(ZnH)_8]$ (**7H**)	Zn		2.489		2.941		
$[Pt(CdH)_8]$ (**1H**)	Cd		2.682		3.171		
$[Pt(HgH)_8]$ (**8H**)	Hg		2.705		3.191		
$[Mo(CdH)_9(ZnH)_3]$ (**3H**)	Cd	Zn	2.917–2.913	2.658	3.054–3.100	2.922–2.944	4.520
$[Mo(ZnH)_{12}]$ (**9H**)	Zn		2.689		2.827		
$[Mo(CdH)_{12}]$ (**10H**)	Cd		2.919		3.069		
$[Mo(HgH)_{12}]$ (**11H**)	Hg		2.941		3.092		

(**11H**)) (Table 1). In previous studies, we have already shown that the M–Zn internuclear distances in the homoleptic parent systems **4H**, **7H**, and **9H** are very similar to those of the synthesized and structurally characterized compounds $[Pd(ZnCp^*)_4(ZnMe)_4]$, $[Pt(ZnCp^*)_4(ZnMe)_4]$, and $[Mo(ZnCp^*)_3(ZnMe)_9]$. These comparisons show that hydrogen-substituted compounds are reasonable model systems to analyze the M–Zn interactions in the real molecules.[2]

To understand the nature of the M–M′ interactions, we performed molecular-orbital analyses, topological analyses of the electron densities according to the atoms-in-molecules theory (AIM),[15] energy-decomposition analyses (EDA) based on canonical molecular orbitals,[16] and the recently developed EDA-NOCV variation of the EDA, which is based on natural orbitals for chemical valence (NOCV).[17] The latter method makes it possible to estimate the strength of individual orbital interactions. This is particularly important for analyzing molecules that have only low symmetry.

Bonding analysis of the octacoordinated [M(M′H)$_8$]: The homoleptic parent compounds **1H** and **4H**–**8H** have energy-minimum structures that have D_{4d} symmetry, whereas **2H** possesses C_{2v} symmetry (see Figure 3).

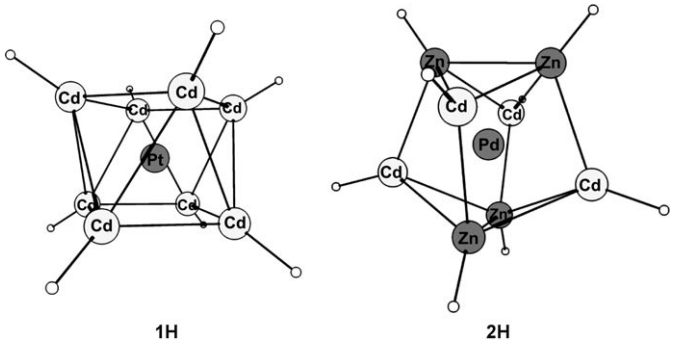

Figure 3. Graphical representations of the energy-minimum structures of the parent compounds $[Pt(CdH)_8]$ (**1H**, D_{4d}) and $[Pd(CdH)_4(ZnH)_4]$ (**2H**, C_{2v}).

The Laplacian distributions $\nabla^2\rho(r)$ of **1H**, **2H**, **5H**, and **6H** are shown in Figure 4 as illustrative examples for the octacoordinated compounds. It becomes clear that there are M–M′ bond paths between the central atom M and the ligand atoms M′ but there are no M′–M′ bond paths between the ligand atoms M′. The same result was previously found for the analogous compounds with zinc as ligand atoms.[2] The AIM results of the other octacoordinated species **4H**, **7H**, and **8H** also do not reveal M′–M′ bond paths.

Although the investigated molecules in this work belong to different point groups and thus different irreducible representations of the molecular orbitals appear, the shapes of the molecular orbitals (MOs) exhibit very similar features. Figure 5a shows the nine highest-occupied Kohn–Sham MOs of the homoleptic compound **1H** as illustrative examples for

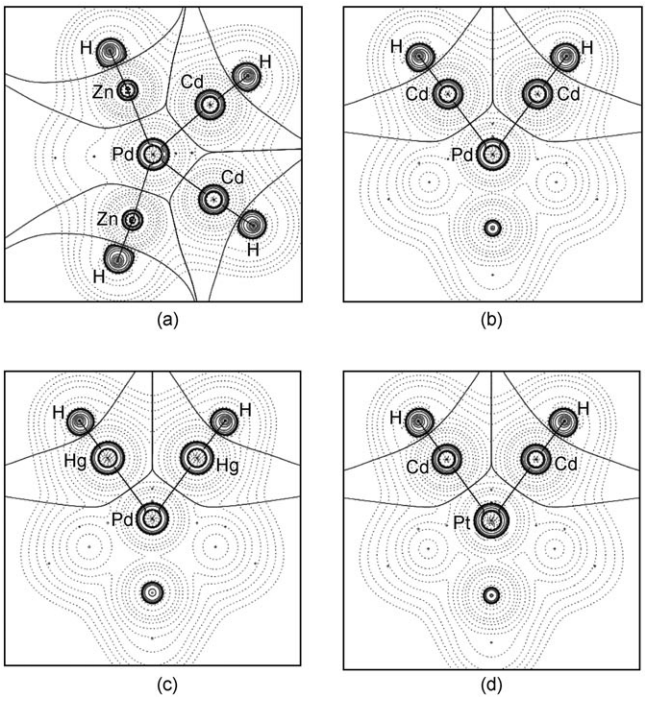

Figure 4. Molecular graphs and contour maps of the Laplacian $\nabla^2\rho(r)$ of a) $Pd(CdH)_4(ZnH)_4]$ (**2H**), b) $[Pd(CdH)_8]$ (**5H**), c) $[Pd(HgH)_8]$ (**6H**), and d) $[Pt(CdH)_8]$ (**1H**).

the parent compounds that possess D_{4d} symmetry. The most important features are shortly discussed. A more extensive discussion is found in our previous study of the zinc complexes.[2] The three highest-lying occupied orbitals represent interactions of the ligand atoms with each other as well as interactions with p atomic orbitals of the central atom.

Since mixing of the s and the d_{z^2} atomic orbitals is allowed in the D_{4d} point group, four of the lower-lying six MOs show mixing of atomic d orbitals with the ligand atoms ($11e_2$ and $11e_3$). Two other orbitals ($10a_1$ and $9a_1$) have both s and d_{z^2} contributions from the metal. The Kohn–Sham MOs of the heteroleptic complex **2H** are presented in Figure 5b. The situation is similar to the homoleptic case **1H**; the three highest-lying MOs have small p atomic orbital (AO) contributions of the central Pd atom, next is an MO with larger s AO contributions, followed by five MOs that represent the mixing of the ligand orbitals with the d AOs of the central atom. Energy-decomposition analyses of **1H** and **4H**–**8H** in D_{4d} symmetry were performed using the EDA method for the interactions of the central atoms in the electronic d^{10} singlet state with the $(M'H)_8$ fragment in the corresponding singlet state. The results are presented in Table 2. The orbital term ΔE_{orb} contributes between 22–28% of the total attractive interactions. The most important contributions to the ΔE_{orb} term come from orbitals that have a_1, e_2, and e_3 symmetry, which comes from metal–ligand bonding of the s and d AOs of the central atom. This holds for all homoleptic compounds **1H** and **4H**–**8H**. For systems that have the same central atom, the magnitude of the interaction energy (ΔE_{int}), Pauli repulsion (ΔE_{Pauli}), electrostatic energy

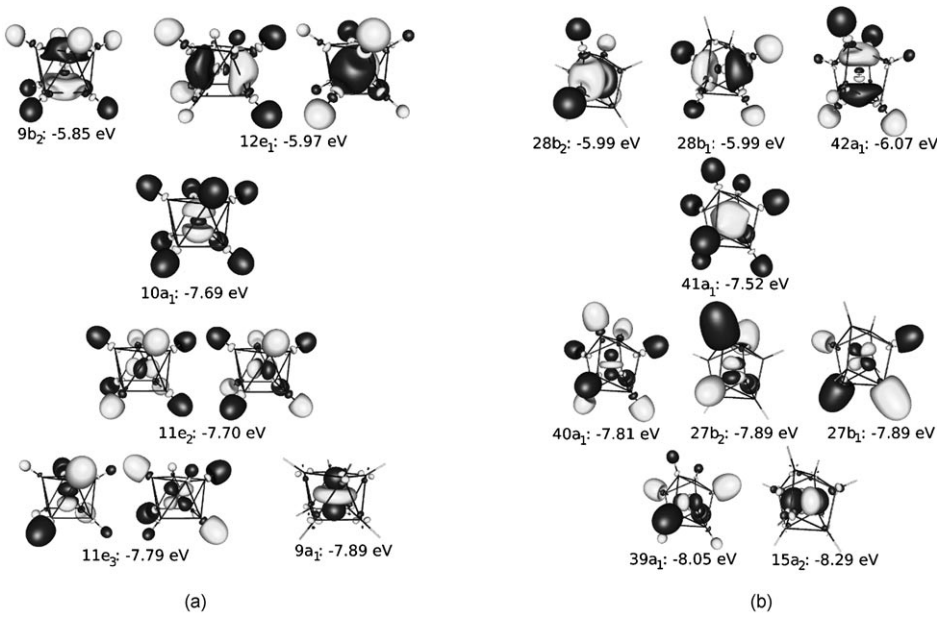

Figure 5. Plot of the nine highest-occupied Kohn–Sham molecular orbitals of a) $[Pt(CdH)_8]$ (**1H**) and b) $[Pd(CdH)_4(ZnH)_4]$ (**2H**).

Table 2. EDA results of $[M(M'H)_8]$ (M = Pd, Pt; M′ = Zn, Cd, Hg) at the BP86/TZ2P+ level. Fragments are M in the $ns^0(n-1)d^{10}$ state and $(M'H)_8$ in the corresponding $^1A_1$ singlet state. Energies in kcal mol^{-1}.

	$[Pd(ZnH)_8]$ (**4H**)		$[Pd(CdH)_8]$ (**5H**)		$[Pd(HgH)_8]$ (**6H**)	
ΔE_{int}	−201.2		−179.7		−185.3	
ΔE_{Pauli}	402.4		344.1		368.3	
ΔE_{elstat}	−467.7	(77.5%)	−404.7	(77.3%)	−408.8	(73.9%)
ΔE_{orb}	−135.8	(22.5%)	−119.2	(22.8%)	−144.7	(26.1%)
$\Delta E(a_1)$ (s, d_{z^2})	−21.7	(16.0%)	−20.5	(17.2%)	−19.9	(13.8%)
$\Delta E(b_2)$ (p_z)	−5.4	(4.0%)	−5.6	(4.7%)	−6.2	(4.3%)
$\Delta E(e_1)$ (p_x, p_y)	−11.0	(8.1%)	−11.2	(9.4%)	−12.3	(8.5%)
$\Delta E(e_2)$ (d_{xy}, $d_{x^2-y^2}$)	−43.6	(32.1%)	−35.8	(30.1%)	−43.2	(29.9%)
$\Delta E(e_3)$ (d_{xz}, d_{yz})	−54.1	(39.8%)	−46.0	(38.6%)	−63.1	(43.6%)
	$[Pt(ZnH)_8]$ (**7H**)		$[Pt(CdH)_8]$ (**1H**)		$[Pt(HgH)_8]$ (**8H**)	
ΔE_{int}	−279.0		−249.1		−254.1	
ΔE_{Pauli}	486.0		413.1		438.9	
ΔE_{elstat}	−583.4	(76.3%)	−498.5	(75.3%)	−500.0	(72.2%)
ΔE_{orb}	−181.6	(23.7%)	−163.8	(24.7%)	−193.0	(27.9%)
$\Delta E(a_1)$ (s, d_{z^2})	−43.8	(24.1%)	−42.9	(26.2%)	−42.1	(21.8%)
$\Delta E(b_2)$ (p_z)	−8.2	(4.5%)	−8.2	(5.0%)	−8.8	(4.5%)
$\Delta E(e_1)$ (p_x, p_y)	−16.7	(9.2%)	−16.5	(10.1%)	−18.0	(9.3%)
$\Delta E(e_2)$ (d_{xy}, $d_{x^2-y^2}$)	−51.2	(28.2%)	−42.7	(26.1%)	−51.9	(26.9%)
$\Delta E(e_3)$ (d_{xz}, d_{yz})	−61.7	(34.0%)	−53.5	(32.7%)	−72.2	(37.4%)

(ΔE_{elstat}), and ΔE_{orb} is largest for the zinc and smallest for the cadmium compounds. Energy contributions of the mercury molecules are slightly larger than those of the cadmium compounds. Note that the strength of the overall interaction energy ΔE_{int} follows the trend Zn > Hg > Cd for the ligand atoms. The platinum complexes have significantly stronger metal–ligand bonds than the palladium species.

It is not possible to distinguish between the contributions of electron donation of the cage to the empty s orbital of the central atom and the backdonation of the d_{z^2} AO to the cage because they belong to the same irreducible representation. Therefore we performed EDA-NOCV analyses for the molecules **1H**, **4H**, and **5H**, which have D_{4d} symmetry, and for **2H**, which has C_{2v} symmetry, to distinguish between individual orbital interactions that have the same symmetry. The numerical results are given in Table 3. A graphical display of the NOCV deformation densities in $[Pd(CdH)_8]$ (**5H**), which is helpful for the understanding of the numerical results, is given in Figure 6. These deformation densities represent the individual orbital interactions.

The NOCV deformation densities show the electron-density change in one NOCV pair upon creating the final molecule during orbital relaxation of the promolecule. Each of these NOCV pairs contains one NOCV with negative eigenvalue v_-, which is an antibonding combination of the fragment orbitals, and one NOCV with positive eigenvalue v_+, which is the corresponding bonding combination. The shape of the deformation densities makes it possible to correlate each NOCV pair with a particular interaction of ligand orbitals with the central AOs of the Pd atom. In the case of the homoleptic complex **5H** (Figure 6), the shapes of the AOs of the central atoms are easy to identify. Thus, the NOCV pairs 1, 2, 4, 5, and 9 represent interactions of the five d AOs of the Pd atom with the Cd ligands; the NOCV pair 3 represents the interaction with the s AO; and the pairs 6, 7, and 8 represent interactions with the p AOs.

The deformation densities show the electron flow of donation and backdonation as it was expected from the choice of the fragments. The ligands donate electron density to the empty p and s AOs of the Pd atom, whereas the occupied d orbitals carry out backdonation to the ligands. The orbital contributions according to the EDA-NOCV analyses are in good agreement with those of the EDA in the framework of canonical MOs as given in Table 2 but give further insight into the bonding situation. The NOCV pairs 3 (s AO of Pd) and 9 (d_{z^2} AO of Pd) correspond to the a_1 irreducible representation of the D_{4d} point group. According to the EDA-

Table 3. EDA-NOCV results of the compounds **1H**, **2H**, **4H**, and **5H**. Fragments are Pd and Pt in the ns^0-$(n-1)d^{10}$ state and $(M'H)_8$ in the corresponding $^1A_1$ singlet state. Energies in kcal mol^{-1}. See Figures 7 and 8 for graphical representations of NOCV pairs and deformation densities.

	$[Pd(ZnH)_8]$ (**4H**)		$[Pd(ZnH)_4(CdH)_4]$ (**2H**)		$[Pd(CdH)_8]$ (**5H**)		$[Pt(CdH)_8]$ (**1H**)	
ΔE_{int}	−201.2		−190.4		−179.7		−249.1	
ΔE_{Pauli}	402.4		379.4		344.1		413.1	
ΔE_{elstat}[a]	−467.7	(77.5 %)	−441.1	(77.5 %)	−404.7	(77.3 %)	−498.5	(75.3 %)
ΔE_{orb}[a]	−135.8	(22.5 %)	−128.4	(22.5 %)	−119.2	(22.8 %)	−163.8	(24.7 %)
1	−27.2	(d)	−24.8	(d)	−22.7	(d)	−32.4	(s)
2	−27.2	(d)	−16.0	(s, d)	−22.7	(d)	−26.5	(d)
3	−11.5	(s)	−22.6	(d)	−12.7	(s)	−26.5	(d)
4	−21.8	(d)	−22.5	(d)	−17.5	(d)	−20.8	(d)
5	−21.8	(d)	−16.5	(s, d)	−17.5	(d)	−20.8	(d)
6	−5.4	(p)	−5.4	(p)	−5.5	(p)	−10.6	(d)
7	−5.4	(p)	−5.5	(p)	−5.3	(p)	−7.7	(p)
8	−5.4	(p)	−5.5	(p)	−5.3	(p)	−7.5	(p)
9	−10.5	(d)	−8.2	(d)	−7.7	(d)	−7.5	(p)

[a] Values in parentheses give the percentage contributions to the total attractive interactions $\Delta E_{elstat} + \Delta E_{orb}$.

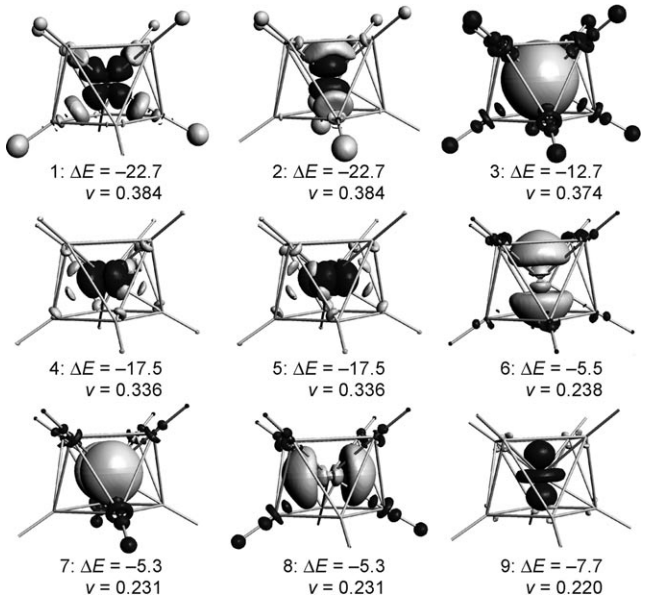

Figure 6. Plot of the NOCV deformation densities of $[Pd(CdH)_8]$ (**5H**). Numbers give the corresponding NOCV eigenvalues v and orbital energy contributions. Light gray isosurfaces indicate areas of charge accumulation, whereas dark gray isosurfaces indicate areas of charge depletion.

NOCV results, the pairs 3 and 9 together contribute −20.4 kcal mol^{-1} to the orbital interactions (3: −12.7 kcal mol^{-1}, 9: −7.7 kcal mol^{-1}), whereas the EDA for the equivalent canonical MOs gives −20.5 kcal mol^{-1} for the irreducible representation a_1. With the EDA-NOCV results, it is possible to distinguish between the donation, which is given by the NOCV pair 3, and backdonation, which is represented by NOCV pair 9.

Adding the contributions of the donation to the p AOs in the EDA-NOCV gives −16.1 kcal mol^{-1}, whereas adding the b_2 and e_1 contributions in EDA give −16.8 kcal mol^{-1}, which is also in good agreement. The same holds for the sum of the NOCV pairs 1, 2, 4, and 5 (−80.4 kcal mol^{-1}) in comparison with the contributions of the e_2 and e_3 irreducible representations in the EDA (−81.8 kcal mol^{-1}). Thus, the EDA-NOCV analysis gives the same results as the EDA but it allows further insight into the bonding situation, even in molecules with high symmetry.

The assignments of NOCV pair contributions to the total orbital interactions for the other investigated homoleptical compounds **1H** and **4H** are given in Table 3. Graphical representations of the deformation densities are given in Figures S1 and S2 in the Supporting Information. The values for the energy contributions ΔE_{int}, ΔE_{Pauli}, ΔE_{elstat}, and ΔE_{orb} provided by the EDA-NOCV analyses agree with those given by the EDA. As for **5H**, summing the EDA-NOCV orbital energy contributions in the same way as discussed above gives good agreement with the EDA orbital energy contributions of the irreducible representations, but with the EDA-NOCV it is possible to distinguish between donation into the vacant s AO of the central atom and backdonation from the d_{z^2} AO. With −32.4 kcal mol^{-1} the donation to the vacant s AO of Pt is larger than the same interaction in the Pd compounds (−12.7 kcal mol^{-1} in **5H**), whereas backdonation from the d AOs to the cage has a similar strength.

Figure 7 shows the graphical representations of the deformation densities in the Zn/Cd heteroleptic compound [Pd-

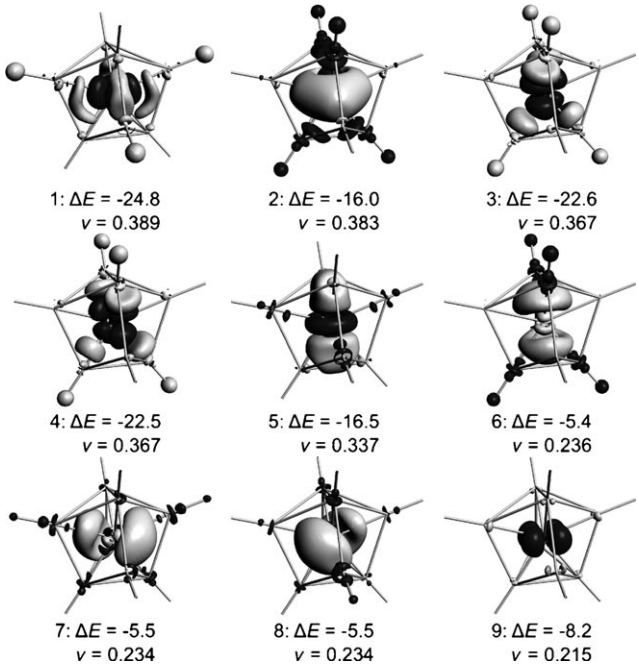

Figure 7. Plot of the NOCV deformation densities of $[Pd(CdH)_4(ZnH)_4]$ (**2H**). Numbers give the corresponding NOCV eigenvalues v and orbital energy contributions. Light gray isosurfaces indicate areas of charge accumulation, whereas dark gray isosurfaces indicate areas of charge depletion.

$(CdH)_4(ZnH)_4]$ (**2H**). The NOCV pairs 1, 3, 4, and 9 represent interactions of the ligands with d atomic orbitals of the Pd atom; the pairs 6, 7, and 8 those with the p AOs of Pd. Thus, with the EDA-NOCV results it is possible to distinguish between interactions with d and with p AOs, which would not be the case with the EDA. Although it is still not strictly possible to distinguish between interactions with the s and the d_{z^2} AOs of Pd with the ligands, the relative contributions may be estimated from the shape of the NOCV pairs 2 and 5. It becomes obvious that the strongest contribution to the NOCV pair 2 comes from the s AO of Pd, whereas the NOCV pair 5 has the largest contribution from the d_{z^2} AO of Pd.

The bonding situation of the homoleptic Cd and heteroleptic Zn/Cd octacoordinated compounds thus looks similar to that of the zinc compounds $[Pd(ZnCp^*)_4(ZnMe)_4]$ and $[Pt(ZnCp^*)_4(ZnMe)_4]$. The M′–M′ interactions are weak but attractive, which explains the large coordination numbers. The stability of the compounds is mainly caused by strong Pd–M′ and Pt–M′ interactions. The AIM analysis does not give bond paths for the Cd–Cd and Hg–Hg interactions.

The bonding situation in dodecacoordinated [Mo(M′H)$_{12}$]: The homoleptical dodecacoordinated compounds $[Mo(ZnH)_{12}]$ (**9H**), $[Mo(CdH)_{12}]$ (**10H**), and $[Mo(HgH)_{12}]$ (**11H**) have perfect icosahedral energy-minimum structures. The parent compound $[Mo(CdH)_9(ZnH)_3]$ (**3H**) possesses C_{3v} symmetry and has a coordination sphere of a slightly distorted icosahedron (Figure 8).

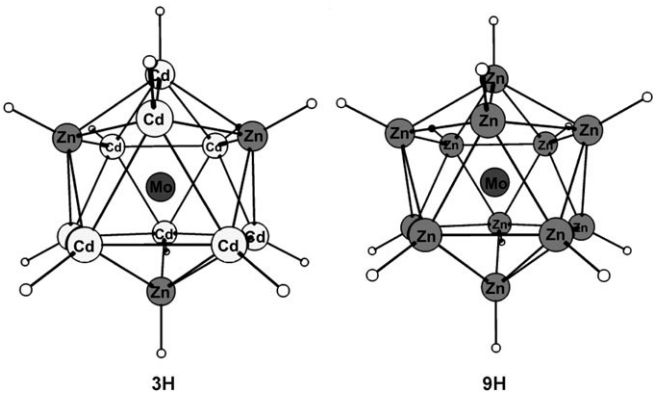

Figure 8. Graphical representations of the minimum structures of the parent compounds $[Mo(CdH)_9(ZnH)_3]$ (**3H**) and $[Mo(ZnH)_{12}]$ (**9H**).

The AIM analyses give Mo–M′ bond critical points but no M′–M′ critical points for M′ = Zn, Cd for **3H**, **9H**, and **10H** (Figure 9a–c). However, in contrast to the dodecacoordinated zinc and cadmium species and to all octacoordinated compounds **1H**, **2H**, **4H**–**8H**, we observe Hg–Hg bond critical points in the mercury compound **11H** (Figure 9d). This finding should not be interpreted, however, as a drastic change in the bonding situation. The curved Hg–Hg bond path suggests the onset of chemical bonding in the definition of the AIM theory. The same observation is made when the

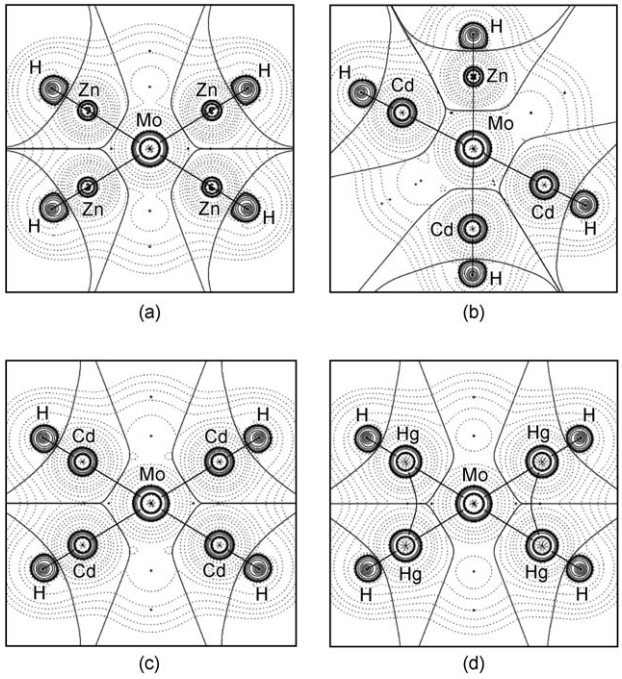

Figure 9. Molecular graphs and contour maps of the Laplacian $\nabla^2\rho$ of a) $[Mo(ZnH)_{12}]$ (**9H**), b) $[Mo(CdH)_9(ZnH)_3]$ (**3H**), c) $[Mo(CdH)_{12}]$ (**10H**), and d) $[Mo(HgH)_{12}]$ (**11H**).

zinc and cadmium compounds are calculated with a slightly distorted geometry in which the M′–M′ distance is a bit shorter than in the equilibrium geometry. The nine highest-lying MOs of the homoleptic complex **10H** are presented in Figure 10. Like in the octacoordinated compounds, and also in the homoleptic zinc compound **9H** that we discussed earlier,[2] the three highest-lying MOs have small p AO contributions of the Mo atom, followed by five atoms with large d AO contributions, and one AO with s AO contributions of the central atom. The frontier orbitals of the icosahedral parent compounds are the triply degenerated t_{1u}, quintuply degenerated h_g, and the total symmetric a_g MOs. An analogous assignment is possible for the highest-lying occupied MOs of the heteroleptic compound **3H**, in which the mixing of p, d, and s AOs of Mo atoms is allowed because the molecule has lower (C_{3v}) symmetry. Thus, the three highest-lying MOs in **3H** mainly represent interactions with the p AOs of Mo, which are polarized by d AOs (see Figure 11) The $35a_1$ MO, which is the energetically lowest-lying orbital from the set of nine MOs, is comparable to the $6a_g$ MO of the perfectly icosahedral compound **10H**.

Energy-decomposition analyses were performed for the three homoleptical icosahedral parent compounds **9H**–**11H**. The results are shown in Table 4. The relative contributions of the orbital interactions ΔE_{orb} to the total interaction energy ΔE_{int} in the dodecacoordinated compounds are larger (39–43%) than in the octacoordinated complexes. The main contributions to ΔE_{orb} come from the h_g orbitals, which represent interactions of the ligands with the singly occupied d orbitals of Mo. The a_g contributions are also

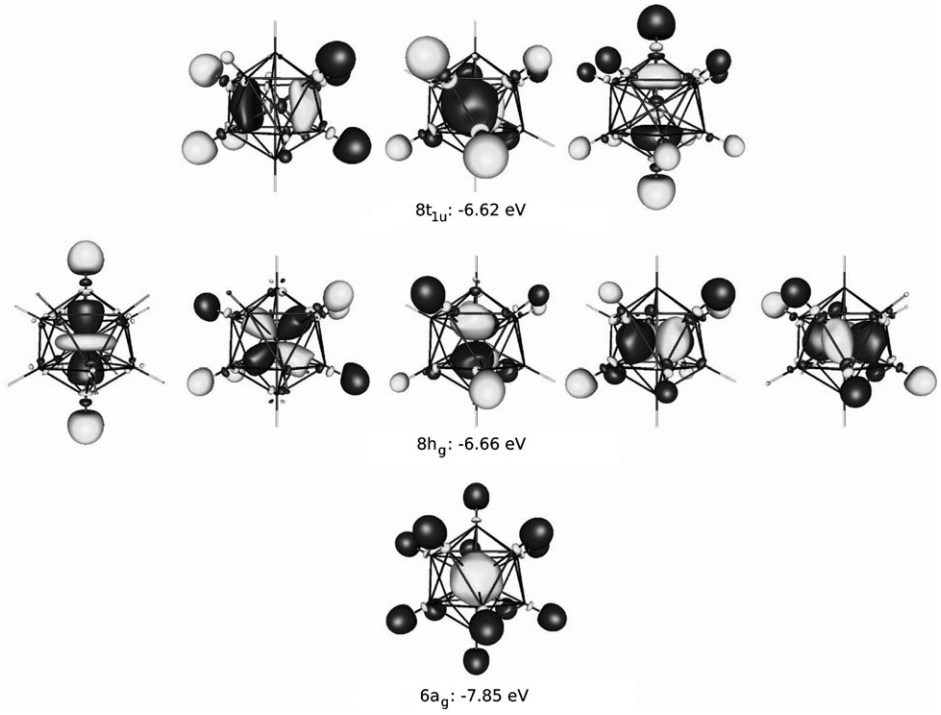

Figure 10. Plot of the nine highest-occupied Kohn–Sham molecular orbitals of $[Mo(CdH)_{12}]$ (**10H**).

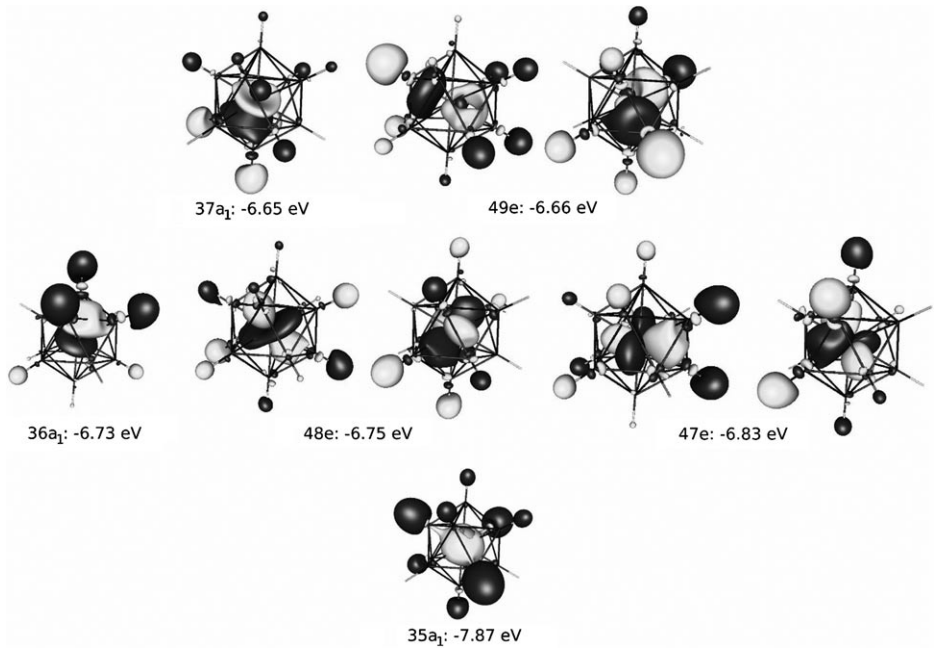

Figure 11. Plot of the nine highest-occupied Kohn–Sham molecular orbitals of $[Mo(CdH)_9(ZnH)_3]$ (**3H**).

quite large, whereas the t_{1u} contributions are negligible as only 40–60% of the total orbital interactions. The strength of the overall interaction energy ΔE_{int} in the dodecahedral complexes **9H**–**11H** shows the same Zn > Hg > Cd trend for the ligand atoms as in the octahedral complexes **4H**–**6H** and **7H**, **1H**, **8H** (Table 2).

Compound **3H**, which has C_{3v} symmetry, has been analyzed with the EDA-NOCV method to distinguish between interactions of s, p, and d AOs of Mo. EDA-NOCV results for **9H** and **10H**, which have I_h symmetry, are given for comparison. The numerical results are shown in Table 5. The values for ΔE_{int}, ΔE_{Pauli}, ΔE_{elstat}, and ΔE_{orb} of the EDA-NOCV results agree with those of the EDA for **9H** and **10H**, as only the decomposition of the orbital term is different in these two approaches. Important insight into the change in the electronic structure of the compounds that derives from the metal–ligand interactions comes from the graphical representations of the deformation densities in the homoleptical complex **10H**, which are given in Figure 12. Because the interacting fragments $Mo + (M'H)_{12}$ in **10H** have open-shell electronic states, it is necessary to distinguish between α and β contributions.

The NOCV pairs 1–6 describe interactions of the $(M'H)_{12}$ fragment with s and d AOs of Mo; pairs 7–9 represent donation from the t_{1u} MOs of $(M'H)_{12}$ to the p AOs of MO. We calculated the Mo fragment with unpaired α electrons and the $(M'H)_{12}$ fragment with unpaired β electrons. Thus, α-NOCV pairs 1–6 describe stabilizations of the s and d electrons of Mo, whereas the corresponding β-NOCV pairs 1–6 describe stabilizations of the a_g and h_g electrons of $(M'H)_{12}$. The corresponding α-NOCV eigenvalues of these NOCV pairs describe the donation of s and d electrons to $(M'H)_{12}$, and the β-NOCV eigenvalues describe donation to Mo.

This is indicated in Figure 12 by the different shading for the deformation densities. For the NOCV pairs that describe interactions with p orbitals of Mo, both α and β contributions describe donation to the p AOs because in this case the interacting orbitals are doubly occupied (t_{1u} of the

Table 4. Results of EDAs of $[Mo(M'H)_{12}]$ ($M'=Zn$, Cd, Hg) at the BP86/TZ2P+ level. Fragments are Mo in the $[Kr]5s^14d^5$ state and $(M'H)_{12}$ in the corresponding ^7A_g septet state. Energies in kcal mol^{-1}.

	$[Mo(ZnH)_{12}]$ (**9H**)		$[Mo(CdH)_{12}]$ (**10H**)		$[Mo(HgH)_{12}]$ (**11H**)	
ΔE_{int}	−348.8		−307.9		−328.7	
ΔE_{Pauli}	594.5		514.1		567.5	
ΔE_{elstat}[a]	−540.1	(57.2%)	−492.5	(59.9%)	−539.3	(60.2%)
ΔE_{orb}[a]	−403.2	(42.8%)	−329.6	(40.1%)	−356.8	(39.8%)
$\Delta E(a_g)$ (s)[b]	−96.4	(23.9%)	−85.1	(25.9%)	−89.7	(25.2%)
$\Delta E(h_g)$ (d)[b]	−288.0	(71.5%)	−227.2	(69.0%)	−247.1	(69.4%)
$\Delta E(t_{1u})$ (p)[b]	−18.3	(4.5%)	−16.9	(5.1%)	−19.5	(5.5%)

[a] Percentage values in parentheses give the percentage contributions to the total attractive energy $\Delta E_{elstat}+\Delta E_{orb}$. [b] Percentage values in parentheses give the percentage contributions to the total orbital interactions ΔE_{orb}.

Table 5. Results of EDA-NOCV analyses of **3H**, **9H**, and **10H** at the BP86/TZ2P+ level. Fragments are Mo in the $[Kr]5s^1d^5$ and $(M'H)_{12}$ ($M'=Zn$, Cd) in the corresponding total symmetric septet state. Energies in kcal mol^{-1}. See Figure 12 and Figure S3 in the Supporting Information for graphical representations of the NOCV deformation densities. Mo was calculated with an excess amount of α, $(M'H)_{12}$ with an excess amount of β.

	$[Mo(ZnH)_{12}]$ (**9H**)		$[Mo(ZnH)_3(CdH)_9]$ (**3H**)		$[Mo(CdH)_{12}]$ (**10H**)	
ΔE_{int}	−349.0		−320.8		−307.9	
ΔE_{Pauli}	594.6		542.7		514.1	
ΔE_{elstat}[a]	−540.1	(57.2%)	−511.6	(59.2%)	−492.5	(59.9%)
ΔE_{orb}[a]	−403.5	(42.8%)	−351.9	(40.8%)	−329.6	(40.1%)
	α	β	α	β	α	β
1	−94.2 (s)	−17.8 (d)	−84.5 (s)	−17.3 (d)	−81.4 (s)	−16.7 (d)
2	−39.8 (d)	−17.8 (d)	−32.4 (d)	−19.0 (d)	−28.4 (d)	−16.7 (d)
3	−39.8 (d)	−17.8 (d)	−32.4 (d)	−19.0 (d)	−28.4 (d)	−16.7 (d)
4	−39.8 (d)	−17.8 (d)	−30.3 (d)	−16.1 (d)	−28.4 (d)	−16.7 (d)
5	−39.8 (d)	−17.8 (d)	−31.3 (d)	−16.1 (d)	−28.4 (d)	−16.7 (d)
6	−39.8 (d)	−2.3 (s)	−31.3 (d)	−2.7 (s)	−28.4 (d)	−3.1 (s)
7	−3.1 (p)	−1.5 (p)	−3.0 (p)	−1.4 (p)	−3.0 (p)	−1.4 (p)
8	−3.1 (p)	−1.5 (p)	−2.9 (p)	−1.4 (p)	−3.0 (p)	−1.4 (p)
9	−3.1 (p)	−1.5 (p)	−2.9 (p)	−1.4 (p)	−3.0 (p)	−1.4 (p)
sum (s)	−96.5	(23.9%)	−87.2	(24.8%)	−84.5	(25.6%)
sum (d)	−288.0	(71.4%)	−245.2	(69.7%)	−225.5	(68.4%)
sum (p)	−13.8	(3.4%)	−13.0	(3.7%)	−13.2	(4.0%)
remain	−5.2	(1.2%)	−6.5	(1.8%)	−6.4	(1.9%)

[a] Values in parentheses give the percentage contributions to the total attractive interactions $\Delta E_{elstat}+\Delta E_{orb}$.

$(M'H)_{12}$ fragment) or vacant (p AOs of the Mo atom). In the case of **10H**, an assignment of the NOCV deformation densities and the corresponding energies to the interactions of $(M'H)_{12}$ orbitals with s, p, or d AOs of Mo are straightforward. This is because there are—for both α and β densities—a set of quintuply degenerated NOCV pairs that represent interactions with d AOs of Mo, a set of triply degenerated NOCV pairs that represent interactions with p AOs of Mo, and one remaining NOCV pair that represents interactions with the s AO of Mo. The latter interaction is represented by the α-NOCV pair 1, which contributes −81.4 kcal mol^{-1} of orbital interactions, and the β-NOCV pair 6, which contributes −3.1 kcal mol^{-1}. The α pair donates the s electron of the central atom to the singly occupied a_g orbital of the $(M'H)_{12}$ fragment, whereas the β pair donates the a_g electron of the $(M'H)_{12}$ fragment to the singly occupied s AO of Mo. Thus, the orbital-stabilization energies of the two electrons differ drastically; the s electron of Mo is much more strongly stabilized upon bond formation than the a_g electron of the $(M'H)_{12}$ fragment. The reason for this large difference is that the s AO of Mo is very compact in comparison to the a_g fragment orbital which is delocalized over the whole $(M'H)_{12}$ moiety.

The sum of the energy contributions of α-pair 1 and β-pair 6, both of which represent interactions with the s AO of Mo, is −84.5 kcal mol^{-1}, which is in good agreement with the a_g contribution of −85.1 kcal mol^{-1} calculated by the EDA method. The sum of the EDA-NOCV contributions of all the NOCV pairs that describe interactions with d AOs of Mo, which is 225.5 kcal mol^{-1}, is also in good agreement with the value of 227.2 kcal mol^{-1} as calculated from the EDA.

The correlation of deformation densities with the interactions of the ligands with the s, p, and d orbitals of Mo in the homoleptic $[Mo(ZnH)_{12}]$ (**9H**) are straightforward. The assignments are given in Table 5, and the graphical representations of the deformation densities are presented in Figure S3 of the Supporting Information. The trends are the same as discussed for **10H**. Again, the overall agreement of EDA-NOCV and EDA results is good. The deformation densities that are associated with the metal–ligand interactions of the $(M'H)_{12}$ fragment orbitals with s, p, and d AOs of Mo in the heteroleptical complex **3H** that come from the EDA-NOCV calculations are shown in Figure S4. The interpretation of the orbital contributions follows the assignments that are given in Table 5.

*Summary of the bonding analysis of **1H–11H***: The detailed bonding analyses using various charge- and energy-decomposition analyses of **1H–11H** suggest that the complexes that are described in this work exhibit different variations of the bonding situation that are characteristic for a new class of compounds. The metal–ligand bonding in the compounds $[M(M'R)_n]$ in which $n=8$ comes mainly from classical donor–acceptor bonding M–M′, which can be described by the Dewar–Chatt–Duncanson model, whereas systems with $n=12$ have electron-sharing bonds augmented by weak additional contributions that come from donor–acceptor interactions. This explains why all examples that were found so far to be stable obey the 18-electron rule. A weaker bonding is found for the interactions between the metal–ligand atoms M′, which arises from orbital interactions that yield

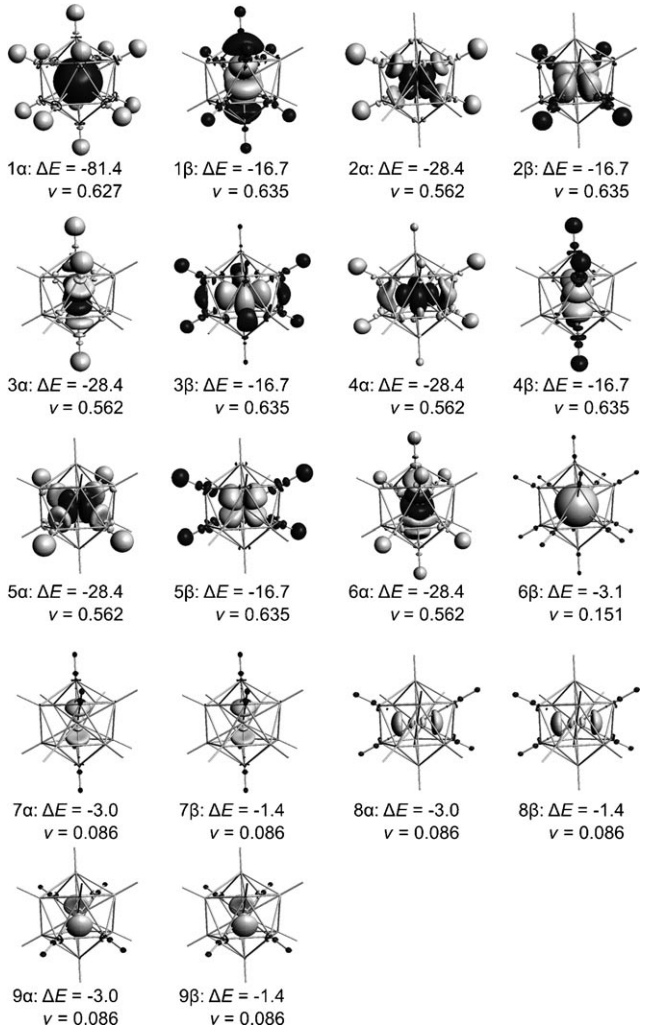

Figure 12. Plot of the α- and β-NOCV deformation densities of $[Mo(CdH)_{12}]$ (**10H**). Numbers give eigenvalues v of the corresponding NOCV pairs and energy contributions (kcal mol^{-1}) to the total orbital energy according to EDA-NOCV. Light gray isosurfaces indicate areas of charge accumulation, whereas dark gray isosurfaces indicate areas of charge depletion.

genuine chemical M′–M′ bonding. The latter attraction may or may not yield bond paths in the AIM calculations but it comes clearly to the fore by inspection of the molecular orbitals. The ligand "cage" fragment $(M'R)_n$ may consist of different atom types M′ as long as the total number of electrons that are donated plus the valence electrons of M gives a total number of 18. The atoms M′ must also be able to engage in weak M′–M′ bonding interactions, which contributes to some extent to the overall binding energy and counterbalances steric repulsion among the ligands. The analysis of the electronic structures thus reveals a unique bonding situation in the $[M(M'R)_n]$ compounds that is clearly different from an endohedral cluster $M@(M'R)_n$ and supports our previous discussions on this matter.[2] The bonding in $[M(M'R)_n]$ compounds resembles the situation in WAu_{12}, which was first theoretically predicted by Pyykkö and Runeberg[18] and then experimentally observed by Li et al.[19] in 2002. In contrast, these latter compounds are characterized by strong chemical bonding within the cage (tangential) and weaker radial bonding between the central atom M and the atoms of the cage. $[Pt@Pb_{12}]^{2-}$ is an icosahedral endohedral cluster compound that was synthesized and discussed by Eichhorn et al.[20] The $[Pb_{12}]^{2-}$ cage provides 26 valence electrons for cluster bonding, thereby fulfilling the Wade–Mingos rules[21] for icosahedral clusters, and thus indicating that the empty cage is stable by itself and only further stabilized by the insertion of the Pt atom, which is also in agreement with experimental observations.[20b] On the contrary, the hypothetical cages $[M'R]_{12}$ (M = Zn, Cd, Hg) have only 12 valence electrons for cluster bonding and thus do not fulfill the Wade–Mingos rules. Geometry optimizations of the empty cages result in decomposition of the cages, which suggests that they are not stable by themselves and that the central atom is essential for the stabilization of the compounds discussed here. As the addition of the molybdenum atom yields 18 valence electrons, the $[M(M'R)_{12}]$ compounds also do not fulfill the Wade–Mingos rules, thus indicating that these compounds are not endohedral clusters. This is in agreement with the results of our bonding analyses that indicate only weak tangential interactions but strong radial M–M′ bonds and thus indicating that the bonding situation in $[M(M'R)_{12}]$ is entirely different from that in endohedral cluster compounds.

Conclusion

Herein we investigated the extension of the concept of highly coordinated transition-metal compounds $[M(M'R)_n]$ that containing one electron ligand M′R (M′ = Zn, Cd; R = CH_3, Cp*) by the synthesis and characterization of the three novel compounds $[Pt(CdMe)_4(CdCp^*)_4]$ (**1**), $[Pd(CdMe)_4(ZnCp^*)_4]$ (**2**), and $[Mo(ZnCp^*)_3(CdMe)_9]$ (**3**). The results of the quantum-chemical bonding analysis reveal that the hitherto unknown Hg analogues of **1**–**3** and even the icosahedral parent compound $[Mo(HgR)_{12}]$ may be quite stable as well. The strength of the overall interaction energy ΔE_{int} for $[M(M'R)_n]$ follows the trend Zn > Hg > Cd, and the platinum complexes have significantly stronger metal–ligand bonds than the palladium species. The calculations clearly show that the transition-metal–Group 12 metal contacts M–M′ in dodecahedral compounds with eight ligands can be best described as classical donor–acceptor bonds, with these radial interactions being much stronger than the tangential M′–M′ interactions. The icosahedral compounds have mainly electron-sharing bonds between the transition-metal and the ligand atoms, which are supported by weak donation from ligand–ligand bonds thus fulfilling the 18-electron rule. Therefore, it is not necessary that the ligand-metal atoms M′ are of the same type as long as they donate electrons to achieve the total electron count of 18 for the central metal M. Last but not least, we would like to suggest that the novel compounds of the general type $[M(M'R)_n]$ may be useful as molecular precursors for soft chemical synthesis of the re-

spective intermetallic alloys or nanoparticles including metal/metal oxide composites, as was demonstrated for the related organometallic precursor chemistry of some binary M/M′ materials (e.g., M = Co, Ni, Cu; M′ = Zn, Al, and Ga).[22]

Experimental Section

General: All manipulations were carried out with rigorous exclusion of air and moisture under an inert gas atmosphere of purified argon using standard Schlenk and glovebox techniques. Hexane and toluene were thoroughly dried using an MBraun Solvent Purification System. The final H_2O content in all solvents was checked by Karl Fischer titration and did not exceed 5 ppm. GaCp*[23,24] was prepared as previously described. Elemental analyses were performed by the Microanalytical Laboratory of the Ruhr-University Bochum. NMR spectra were recorded using a Bruker Avance DPX-250 spectrometer in C_6D_6 at 298 K. Chemical shifts (δ in ppm) are given relative to TMS and were referenced to the solvent resonances as internal standards, and are consecutively reported as position (δ_H or δ_C), relative integral, multiplicity (s = singlet, d = doublet, sept = septet, m = multiplet), coupling constant (J in Hz), and assignment.

X-ray crystallography: Crystals of **1**, **2**, and **3** were obtained from hexane at −30 °C. The X-ray diffraction intensities were collected using an Oxford Xcalibur2 diffractometer with a Sapphire2 CCD. The crystal structures were solved by direct methods using SHELXS-97 and refined with SHELXL-97.[25] The crystals were coated with a perfluoropolyether, picked up with a glass fiber, and immediately mounted in the cooled nitrogen stream of the diffractometer. The crystallographic data and details of the final R values are provided in Table S2 of the Supporting Information. Molecules **1**–**3** were refined with distance restraints and restraints for the anisotropic displacement parameters. Cocrystallized solvent molecules were removed from the diffraction data using PLATON/SQUEEZE.[26,27]

CCDC-777129 (**1**), 777130 (**2**), and 777131 (**3**) contain the supplementary crystallographic data for this paper. These data can be obtained free of charge from The Cambridge Crystallographic Data Centre via www.ccdc.cam.ac.uk/data_request/cif.

[Pt(CdMe)$_4$(CdCp*)$_4$] (1): A sample of [Pt(GaCp*)$_4$][28] (0.100 g, 0.099 mmol) in toluene (6 mL) was cooled to −30 °C and treated with $CdMe_2$ (0.119 g, 0.835 mmol). The reaction mixture was warmed to room temperature and stirred for 30 min. The solvent was removed under vacuum and the crude product was extracted with hexane. The product crystallized by slow cooling to −30 °C. Yield: 0.079 g (47 %). ^{1}H NMR (C_6D_6, 25 °C): δ = 2.19 (60 H; C_5Me_5), 0.03 ppm (12 H; CdMe); ^{13}C NMR (C_6D_6, 25 °C): δ = 112.21 (C_5Me_5), 19.72 (CdMe), 11.03 ppm (C_5Me5); elemental analysis calcd (%) for $C_{44}H_{72}Cd_8Pt$: C 31.17, H 4.28; found: C 31.18, H 4.13.

[Pd(CdMe)$_4$(ZnCp*)$_4$] (2): A sample of [Pd(ZnCp*)$_4$(ZnMe)$_4$][2] (100 mg; 0.081 mmol) in hexane (6 mL) was treated with $CdMe_2$ (226 mg; 1.586 mol). The reaction mixture was warmed to 60 °C for 30 min. The solution was filtered and the solvent was removed under vacuum. The crude product was redissolved in hexane. The product crystallized by slow cooling to −30 °C. Yield: 0.056 g (48 %). ^{1}H NMR (C_6D_6, 25 °C): δ = 2.08 (60 H; C_5Me_5), 0.14 ppm (12 H; CdMe); ^{13}C NMR (C_6D_6, 25 °C): δ = 110.54 (C_5Me_5), 19.72 (CdMe), 10.93 ppm (C_5Me_5); elemental analysis calcd (%) for $C_{44}H_{72}Cd_4Zn_4Pd$: C 37.25, H 5.11; found: C 37.36, H 5.56.

[Mo(ZnCp*)$_3$(CdMe)$_9$] (3): A sample of [Mo(ZnCp*)$_4$(GaMe)$_4$][2] (70 mg; 0.057 mmol) in hexane (5 mL) was treated with a 14-fold molar excess amount of $CdMe_2$ (160 mg; 1.123 mol) at room temperature. The reaction mixture was warmed to 60 °C for 30 min. The solution was filtered and the solvent was removed under vacuum. The crude product was redissolved in hexane. The product crystallized by slow cooling to −30 °C. Yield: 0.035 g (33 %). ^{1}H NMR (C_6D_6, 25 °C): δ = 2.17 (45 H; C_5Me_5), 0.33 (9 H; CdMe); 0.21 (9 H; CdMe); 0.15 ppm (9 H; CdMe); ^{13}C NMR (C_6D_6, 25 °C): δ = 114.16 (C_5Me_5), 31.13 (CdMe), 29.38 (CdMe), 27.19 (CdMe), 11.14 ppm (C_5Me_5); elemental analysis calcd (%) for $C_{39}H_{72}Cd_9Zn_3Mo$: C 25.39, H 3.93, Zn 10.63; found: C 26.19, H 3.90, Zn 10.91.

Computational details: The geometries of the molecules were optimized at the gradient-corrected DFT level of theory using Becke's exchange functional[29] in conjunction with Perdew's correlation functional[30] (BP86) with the TURBOMOLE 5.80 program package.[31] Ahlrich's def2-TZVPP basis set[32] was used. The RI approximation[33] was applied using auxiliary basis functions.[34] Stationary points were characterized by the analytical calculation of the Hessian using the aoforce module in TURBOMOLE.[35] This level of theory is denoted as RI-BP86/def2-TZVPP. Energy-decomposition analyses (EDA) were carried out using the ADF(2009.1) program package.[36] Uncontracted Slater-type orbitals (STOs) were employed as basis functions in self-consistent field (SCF) calculations.[37] Triple-zeta-quality basis sets were used, which were augmented by two sets of polarization functions, that is, p and d functions for the hydrogen atom and d and f functions for the other atoms. This level of theory is denoted as BP86/TZ2P+. An auxiliary set of s, p, d, f, and g STOs was used to fit the molecular densities and to represent the Coulomb and exchange potentials accurately in each SCF cycle.[38] Scalar relativistic effects were considered using the zero-order regular approximation (ZORA).[39] In the EDA, bond formation between the interacting fragments is divided into three steps, which can be interpreted in a plausible way. In the first step, the fragments, which are calculated with the frozen geometry of the entire molecule, are superimposed without electronic relaxation to yield the quasiclassical electrostatic attraction ΔE_{elstat}. In the second step, the product wave function becomes antisymmetrized and renormalized, which gives the repulsive term ΔE_{Pauli}, termed Pauli repulsion. In the third step, the molecular orbitals relax to their final form to yield the stabilizing orbital interaction ΔE_{orb}. The latter term can be divided into contributions of orbitals that have different symmetry (in the EDA) or into contributions of NOCV orbital pairs (EDA-NOCV). These latter steps are crucial for the present study. The sum of the three terms $\Delta E_{elstat} + \Delta E_{Pauli} + \Delta E_{orb}$ gives the total interaction energy ΔE_{int}. Note that ΔE_{int} is not the same as the bond-dissociation energy, because the relaxation of the fragments is not considered in ΔE_{int}. The interaction energy, ΔE_{int}, together with the term ΔE_{prep}, which is the energy necessary to promote the fragments from their equilibrium geometry to the geometry in the compounds, can be used to calculate the bond-dissociation energy as $-D_e = \Delta E_{prep} + \Delta E_{int}$. Because we are not concerned with the bond-dissociation energies in this paper, we give only the values for ΔE_{int} and its contributing terms. Further details about the EDA and the EDA-NOCV can be found in the literature.[16,17,40,41]

Acknowledgements

T.B. is grateful for a PhD scholarship by the Fonds der Chemischen Industrie (Germany) and for support by the Ruhr University Research School. Excellent service by the Hochschulrechenzentrum of the Philipps-University Marburg is gratefully acknowledged. Further computer time was obtained from the Centre for Scientific Computing of the Goethe-University Frankfurt. This work was funded by the project "Metal-Rich Molecules" of the German Research Foundation (DFG, Fi-502/24-1).

[1] a) S. Gonzalez-Gallardo, G. Prabusankar, T. Cadenbach, C. Gemel, M. von Hopffgarten, G. Frenking, R. A. Fischer, *Struct. Bonding (Berlin)* **2010**, *136*, 147–188; b) P. W. Roesky, *Dalton Trans.* **2009**, 1887–1893; c) H.-J. Himmel, G. Linti, *Angew. Chem.* **2008**, *120*, 6425–6427; *Angew. Chem. Int. Ed.* **2008**, *47*, 6326–6328; d) D. L. Kays, S. Aldridge, *Struct. Bonding (Berlin)* **2008**, *130*, 29–122; e) R. J. Baker, C. Jones, *Coord. Chem. Rev.* **2005**, *249*, 1857–1869; f) C. Gemel, T. Steinke, M. Cokoja, A. Kempter, R. A. Fischer, *Eur. J. Inorg. Chem.* **2004**, 4161–4176; g) G. Linti, H. Schnöckel, *Coord.*

Chem. Rev. **2000**, *206–207*, 285–319; h) R. A. Fischer, J. Weiss, *Angew. Chem.* **1999**, *111*, 3002–3022; *Angew. Chem. Int. Ed.* **1999**, *38*, 2830–2850.

[2] a) T. Cadenbach, C. Gemel, R. A. Fischer, *Angew. Chem.* **2008**, *120*, 9286–9289; *Angew. Chem. Int. Ed.* **2008**, *47*, 9146–9149; b) T. Cadenbach, T. Bollermann, C. Gemel, I. Fernandez, M. von Hopffgarten, G. Frenking, R. A. Fischer, *Angew. Chem.* **2008**, *120*, 9290–9295; *Angew. Chem. Int. Ed.* **2008**, *47*, 9150–9154; c) T. Cadenbach, T. Bollermann, C. Gemel, M. Tombul, I. Fernandez, M. von Hopffgarten, G. Frenking, R. A. Fischer, *J. Am. Chem. Soc.* **2009**, *131*, 16063–16077.

[3] T. F. Fässler, S. D. Hoffmann, *Angew. Chem.* **2004**, *116*, 6400–6406; *Angew. Chem. Int. Ed.* **2004**, *43*, 6242–6248.

[4] M. J. Adrowski, W. R. Mason, *Inorg. Chem.* **1997**, *36*, 1443–1453, and references herein.

[5] a) A. Looney, A. Saleh, Y. Zhang, G. Parkin, *Inorg. Chem.* **1994**, *33*, 1158–1164; b) H. Tang, M. Parvez, H. G. Richey, Jr., *Organometallics* **1996**, *15*, 5281–5283; c) H. Nöth, M. Thomann, *Chem. Ber.* **1995**, *128*, 923–927.

[6] a) L. Arnberg, *Acta Crystallogr. Sect. B* **1980**, *36*, 527–532; b) H. Nowotny, E. Bauer, A. Stempfl, *Monatsh. Chem.* **1950**, *81*, 1164–1164; c) H. Nowotny, E. Bauer, A. Stempfl, *Monatsh. Chem.* **1952**, *83*, 221–236.

[7] T. Yamaguchi, F. Yamazaki, T. Ito, *J. Am. Chem. Soc.* **1999**, *121*, 7405–7406.

[8] J. Forniés, J. Gomez, E. Lalinde, M. T. Moreno, *Inorg. Chem.* **2001**, *40*, 5415–5419.

[9] R. Faggiani, R. J. Gillespie, J. E. Vekris, *Chem. Commun.* **1986**, *7*, 517–518.

[10] T. Steinke, C. Gemel, M. Winter, R. A. Fischer, *Angew. Chem.* **2002**, *114*, 4955–4957; *Angew. Chem. Int. Ed.* **2002**, *41*, 4761–4763.

[11] S. Adam, A. Bauer, O. Timpe, U. Wild, G. Mestl, W. Bensch, R. Schlögl, *Chem. Eur. J.* **1998**, *4*, 1458–1469.

[12] C. M. Fafard, C.-H. Chen, B. M. Foxman, O. V. Ozerov, *Chem. Commun.* **2007**, 4465–4467.

[13] a) D. del Río, A. Galindo, I. Resa, E. Carmona, *Angew. Chem.* **2005**, *117*, 1270; *Angew. Chem. Int. Ed.* **2005**, *44*, 1244–1247; b) Z.-Z. Liu, W. Q. Tian, J.-K. Feng, G. Zhang, W.-Q. Li, Y.-H. Cui, C.-C. Sun, *Eur. J. Inorg. Chem.* **2006**, 2808–2818; c) I. Resa, E. Carmona, E. Gutierrez-Puebla and A. Monge, *Science* **2004**, *305*, 1136–1138.

[14] a) P. Braunstein, M. Knorr, M. Strampfer, A. DeCian, J. Fischer, *Dalton Trans.* **1994**, *2*, 117–134; b) S. Seebald, B. Mayer, U. Schubert, *Inorg. Chem.* **1995**, *34*, 5285–5288.

[15] R. F. W. Bader, *Atoms in Molecules: A Quantum Theory*, Oxford University Press, New York, **1990**.

[16] a) K. Morokuma, *J. Chem. Phys.* **1971**, *55*, 1236–1244; b) T. Ziegler, A. Rauk, *Theor. Chim. Acta* **1977**, *46*, 1–10.

[17] M. P. Mitoraj, A. Michalak, T. Ziegler, *J. Chem. Theory Comput.* **2009**, *5*, 962–975.

[18] P. Pyykkö, N. Runeberg, *Angew. Chem.* **2002**, *114*, 2278–2280; *Angew. Chem. Int. Ed.* **2002**, *41*, 2174–2176.

[19] X. Li, B. Kiran, J. Li, H.-J. Zhai, L.-S. Wang, *Angew. Chem.* **2002**, *114*, 4980–4983; *Angew. Chem. Int. Ed.* **2002**, *41*, 4786–4789.

[20] a) E. N. Esenturk, J. Fettinger, Y.-F. Lam, B. Eichhorn, *Angew. Chem.* **2004**, *116*, 2184–2186; *Angew. Chem. Int. Ed.* **2004**, *43*, 2132–2134; b) E. N. Esenturk, J. Fettinger, B. Eichhorn, *J. Am. Chem. Soc.* **2006**, *128*, 9178–9186.

[21] a) K. Wade, *Adv. Inorg. Chem. Radiochem.* **1976**, *18*, 1–66; b) D. M. P. Mingos, *Acc. Chem. Res.* **1984**, *17*, 311–319.

[22] a) J. Hambrock, M. K. Schroeter, A. Birkner, C. Woll, R. A. Fischer, *Chem. Mater.* **2003**, *15*, 4217–4222; b) M. Cokoja, H. Parala, M. K. Schroter, A. Birkner, M. W. E. van den Berg, K. V. Klementiev, W. Gruenert, R. A. Fischer, *J. Mater. Chem.* **2006**, *16*, 2420–2428; c) M. K. Schroeter, L. Khodeir, M. W. E. van den Berg, T. Hikov, M. Cokoja, S. J. Miao, W. Gruenert, M. Muhler, R. A. Fischer, *Chem. Commun.* **2006**, 2498–2500; d) M. Cokoja, B. R. Jagirdar, H. Parala, A. Birkner, R. A. Fischer, *Eur. J. Inorg. Chem.* **2008**, 3330–3339; e) M. Cokoja, H. Parala, A. Birkner, R. A. Fischer, O. Margeat, D. Ciuculescu, C. Amiens, B. Chaudret, A. Falqui, and P. Lecante, *Eur. J. Inorg. Chem.* **2010**, 1599–1603.

[23] P. Jutzi, B. Neumann, G. Reumann, H.-G. Stammler, *Organometallics* **1998**, *17*, 1305–1314.

[24] P. Jutzi, L. O. Schebaum, *J. Organomet. Chem.* **2002**, *654*, 176–179.

[25] G. M. Sheldrick, *Acta Crystallogr. Sect. A* **2008**, *64*, 112–122.

[26] A. L. Spek, *Acta Crystallogr. Sect. D* **2009**, *65*, 148–155.

[27] P. Van der Sluis, A. L. Spek, *Acta Crystallogr. Sect. A* **1990**, *46*, 194–201.

[28] T. Steinke, C. Gemel, M. Winter, R. A. Fischer, Roland, *Chem. Eur. J.* **2005**, *11*, 1636–1646.

[29] A. D. Becke, *Phys. Rev. A* **1988**, *38*, 3098–3100.

[30] J. P. Perdew, *Phys. Rev. B* **1986**, *33*, 8822–8824.

[31] R. Ahlrichs, M. Bär, M. Häser, H. Horn, C. Kölmel, *Chem. Phys. Lett.* **1989**, *162*, 165–169.

[32] F. Weigend, R. Ahlrichs, *Phys. Chem. Chem. Phys.* **2005**, *7*, 3297–3305.

[33] R. Ahlrichs, *Phys. Chem. Chem. Phys.* **2004**, *6*, 5119–5121.

[34] a) K. Eichkorn, O. Treutler, M. Häser, R. Ahlrichs, *Chem. Phys. Lett.* **1995**, *242*, 652–660; b) K. Eichkorn, F. Weigend, O. Treutler, R. Ahlrichs, *Theor. Chem. Acc.* **1997**, *97*, 119–124; c) F. Weigend, *Phys. Chem. Chem. Phys.* **2006**, *8*, 1057–1065.

[35] P. Deglmann, K. May, F. Furche, R. Ahlrichs, *Chem. Phys. Lett.* **2004**, *384*, 103–107.

[36] ADF2009.01, SCM, Theoretical Chemistry; Vrije Universiteit, Amsterdam, http://www.scm.com.

[37] J. G. Snijders, E. J. Baerends, P. Vernooijs, *At. Nucl. Energy At. Data Nucl. Tables* **1981**, *26*, 483–509.

[38] J. Krijn, E. J. Baerends, *Fit Functions in the HFSMethod, Internal Report*, Vrije Universiteit Amsterdam, Amsterdam, **1984**.

[39] a) C. Chang, M. Pelissier, P. Durand, *Phys. Scr.* **1986**, *34*, 394–404; b) J.-L. Heully, I. Lindgren, E. Lindroth, S. Lundquist, A. M. Mårtensson-Pendrill, *J. Phys. B* **1986**, *19*, 2799–2815; c) E. van Lenthe, E. J. Baerends, J. G. Snijders, *J. Chem. Phys.* **1993**, *99*, 4597–4610; d) E. van Lenthe, E. J. Baerends, J. G. Snijders, *J. Chem. Phys.* **1996**, *105*, 6505–6516; e) E. van Lenthe, R. van Leeuwen, E. J. Baerends, J. G. Snijders, *Int. J. Quantum Chem.* **1996**, *57*, 281–293.

[40] G. te Velde, F. M. Bickelhaupt, E. J. Baerends, S. J. A. van Gisbergen, C. Fonseca Guerra, J. G. Snijders, T. Ziegler, *J. Comput. Chem.* **2001**, *22*, 931–967.

[41] Recent reviews about the EDA method and its application have been published by: a) F. M. Bickelhaupt, E. J. Baerends, *Rev. Comput. Chem.* **2000**, *15*, 1–86; b) M. Lein, G. Frenking, *Theory and Applications of Computational Chemistry: The First 40 Years; Dykstra* (Eds.. G. Frenking, K. S. Kim, G. E. Scuseria), Elsevier, Amsterdam, **2005**, pp. 291–372.

Received: June 10, 2010
Published online: October 11, 2010

